2nd Advanced Optical Metrology Compendium

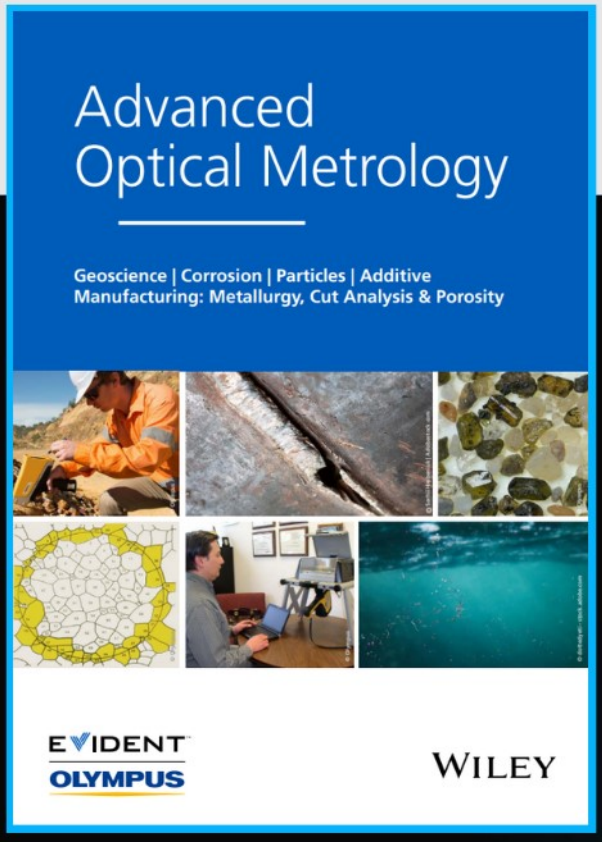

The latest eBook from Advanced Optical Metrology. Download for free.

This compendium includes a collection of optical metrology papers, a repository of teaching materials, and instructions on how to publish scientific achievements.

With the aim of improving communication between fundamental research and industrial applications in the field of optical metrology we have collected and organized existing information and made it more accessible and useful for researchers and practitioners.

EVIDENT
OLYMPUS

WILEY

NANO · MICRO small
www.small-journal.com

3D Nanolithography by Means of Lipid Ink Spreading Inhibition

Eider Berganza, Evgeniy Boltynjuk, George Mathew, Fabio Fernando Vallejo, Roland Gröger, Torsten Scherer, Sylwia Sekula-Neuner, and Michael Hirtz**

While patterning 2D metallic nanostructures are well established through different techniques, 3D printing still constitutes a major bottleneck on the way to device miniaturization. In this work a fluid phase phospholipid ink is used as a building block for structuring with dip-pen nanolithography. Following a bioinspired approach that relies on ink-spreading inhibition, two processes are presented to build 2D and 3D metallic structures. Serum albumin, a widely used protein with an innate capability to bind to lipids, is the key in both processes. Covering the sample surface with it prior to lipid writing, anchors lipids on the substrate, which ultimately allows the creation of highly stable 3D lipid-based scaffolds to build metallic structures.

1. Introduction

Miniaturization of devices[1] and 3D printing of nanoscale-size structures constitute one of the major challenges in nanofabrication nowadays. Sophisticated photonic devices,[2] spintronics,[3] sensing,[4] regenerative medicine,[5] cell engineering[6] or cell fate control[7] represent prominent examples of the different areas that require the creation of active structural units at the nanometer scale.

Despite 2D lithography of metallic nanostructures being very well-established through different techniques (in particular prominent photolithography and electron beam lithography), the creation of micro/nanoscale 3D metallic structures with arbitrary shapes still constitutes a challenge. In this regard, electron and ion beam technologies have proven to be able to write 3D structures with high resolution.[8] A recent publication reports the creation of a Co double helix structure using focus electron beam-induced deposition,[9] although these techniques are not fully established and require the use of expensive equipment. Following a different approach, based on scanning probe lithography (SPL), Hengsteler and coauthors were able to electroplate sub-100 nm diameter copper pillars with the FluidFM technology and created other complex 3D arbitrary shapes.[10] Some authors propose to circumvent the current nanofabrication limitations by metalizing a pre-fabricated 3D scaffold using a two-step fabrication process.[11,12]

Scaffolding can be achieved through additive manufacturing-based strategies, which have endowed the third dimension in macroscale printing. These strategies are currently being translated to nanoscale structuring. While direct laser writing techniques, such as two-photon lithography[13] are powerful candidates to create polymeric scaffolds,[12] SPL techniques are currently been developed to print 3D structures. SPL techniques provide a good alternative to the above-mentioned technologies, as they do not require very expensive facilities or clean rooms to obtain high pattern resolution. It has recently been demonstrated that using the FluidFM technology, a monomer ink can be patterned in a layer-by-layer writing process with intermediate curing steps which can dispense a UV curable polymer[14,15] or a customized polymer to achieve rapid surface-initiated crosslinking through versatile macro-crosslinkers.[16] Alternatively, 3D dip-pen nanolithography (DPN) printing was recently achieved by careful design of a polymer endowing it with a humidity-dependent behavior and adequate rheological properties.[17] While the design of printing inks has been extensively explored, much less effort has been devoted to the design and chemical functionalization of substrates to achieve different effects, such as hampering the ink spreading, due to tailored surface energies,[18] although some authors already stated

E. Berganza
Instituto de Ciencia de Materiales de Madrid (ICMM)
Consejo Superior de Investigaciones Científicas (CSIC)
Sor Juana Ines de la Cruz 3, 29048 Madrid, Spain
E-mail: eider.berganza@csic.es

E. Berganza, E. Boltynjuk, G. Mathew, R. Gröger, T. Scherer, M. Hirtz
Institute of Nanotechnology (INT) & Karlsruhe Nano Micro Facility (KNMF)
Karlsruhe Institute of Technology (KIT)
Hermann-von-Helmholtz-Platz 1 76344, Eggenstein-Leopoldshafen, Germany
E-mail: michael.hirtz@kit.edu

F. F. Vallejo
Departamento de Ingeniería Mecánica y Mecatrónica
Universidad Nacional de Colombia
Cra 45, 111321 Bogotá, Colombia

R. Gröger
Karlsruhe Institute of Technology (KIT)
Institute of Applied Physics (APH)
Wolfgang-Gaede-Straße 1, 76131 Karlsruhe, Germany

S. Sekula-Neuner
n.able GmbH
Hermann-von-Helmholtz-Platz 1, 76344 Eggenstein-Leopoldshafen, Germany

The ORCID identification number(s) for the author(s) of this article can be found under https://doi.org/10.1002/smll.202205590.

DOI: 10.1002/smll.202205590

the importance of combining tailored surface properties with advanced nanofabrication tools.[19]

On another note, DPN with phospholipids (l-DPN) is a well-established technique,[20] where the use of 1,2-dioleoyl-sn-glycero-3-phosphocholine (DOPC) as a carrier ink ensures a smooth, humidity-dependent flow of molecules upon tip-substrate contact. The amount of transferred ink depends on the writing speed, but it can also be tuned by humidity and surface energy. L-DPN was used to pattern surfaces with biomimetic membranes for biomedical experiments,[23–26] or as a carrier to deposit different species.[27]

Depending on the substrate properties, the lipid structures will show different stability and spreading behavior.[29–32] In this work we propose a new bioinspired approach to anchor lipids to the substrate and prevent spreading in order to achieve control on the out-of-plane writing dimension, by introducing a biomolecule that has a high affinity for the phospholipids. We take advantage of this property to 1) implement achieved thick lipid layers as masks for 2D lithography and 2) build 3D scaffolds that can later be metalized.

2. Results and Discussion

Functionalization of the substrates can be crucial to control ink spreading.[15,28] Pre-coated self-assembled monolayers with non-polar head groups are often used on surfaces to prevent lipid spreading diffusion on the surface.[18,31] On the other hand, serum albumin – one of the most abundant proteins in mammalian plasma, with a small size, high stability, and non-reactive nature, commonly used to prevent non-specific binding in immunohistochemistry assays – has been long known for its capability to bind to fatty acids.[33] Two different parts constitute the albumin binding sites: a pocket lined with nonpolar amino acid side chains and a cationic group located at or near the surface of the pocket.[34] Free Fatty Acid binding occurs via hydrophobic interactions with the hydrocarbon chain and electrostatic interactions with the carboxylate anion.

Given that bovine serum albumin (BSA) can be adsorbed on different surfaces and still retain the bioactivity of its binding sites,[35] we can use it to tune the properties of substrates and achieve a lipid anchoring behavior that prevents the spreading of the lipid ink during and after L-DPN (**Figure 1**a). The DOPC phospholipid chosen as ink for lithography is displayed in Figure 1b. After the preparation of BSA-coated silicon substrates (crystal structure shown in Figure 1c), the water contact angle was measured (Figure 1d) and showed a mild hydrophilic behavior (47 ± 2°). Atomic force microscopy (AFM) measurements confirmed that the surface is fully coated with the spherical-shaped BSA protein (Figure 1e) and displayed a roughness below 2 nm.

2.1. 2D Lithography: Using the Lipids as Lithography Masks

Writing tests and comparing the thickness of the lipid patches obtained, show indeed significantly higher structures on these BSA-coated substrates, as compared to other functionalized substrates (Supporting Information S1). This can be attributed to the blocking of lipid spreading, as piling up on top of other phospholipid molecules turns out to be energetically more favorable than spreading to BSA-coated substrate areas. This property enabled writing thick arbitrary shaped lipid patches (e.g., ≈200 nm thick, for standard writing conditions, that is, 40% RH, 1 µm s^{-1} writing speed) and to use them as masks and proceed to further nanolithography steps that translated the lipid structures into any desired material. A two-step lithography process is proposed, where the lipids are used to protect surface areas during physical vapor deposition (PVD) and produce a mold after a lift-off process, followed by a second PVD and lift-off step (see steps on **Figure 2**a–f).

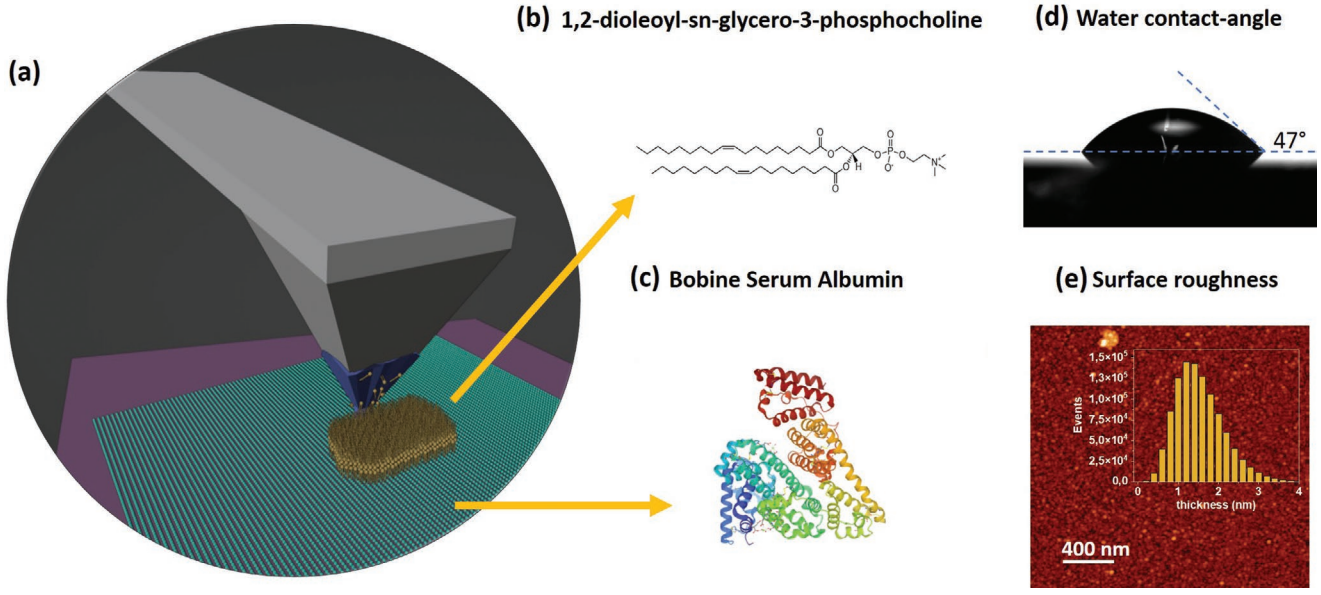

Figure 1. Lipid writing on (BSA) coated surfaces. a) Sketch showing (L-DPN) on a BSA-coated surface. b) Chemical structure of the DOPC lipid molecules used for lithography. c) 3D crystal structure of BSA. d) Water contact angle and e) roughness characterization of a surface with adsorbed BSA.

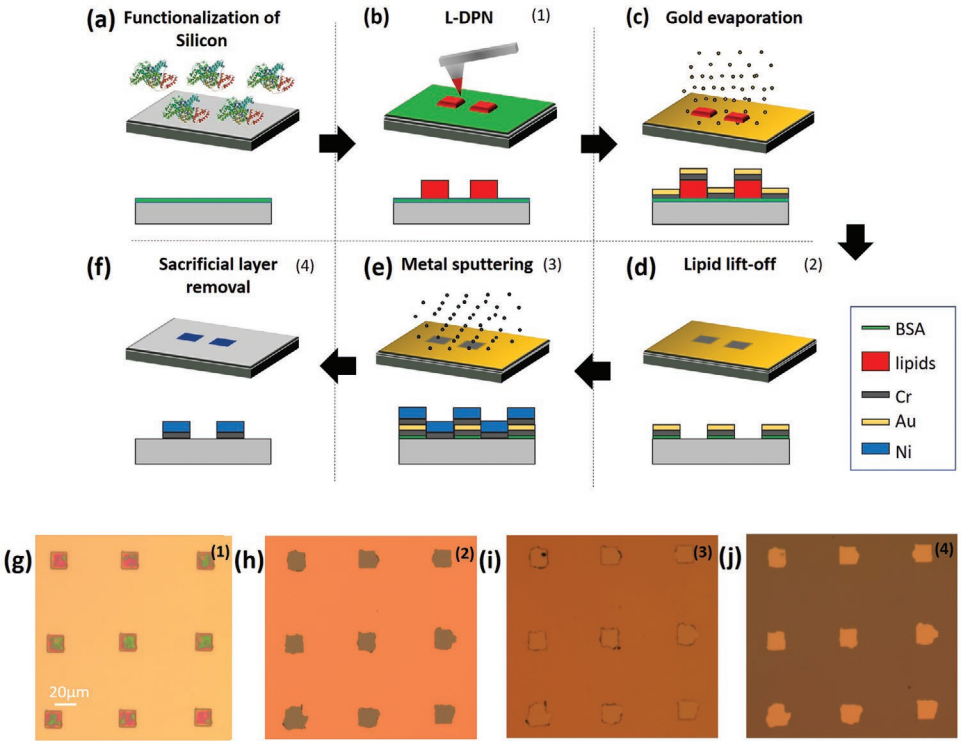

Figure 2. Sketch illustrating the proposed 2D lithography process: a) incubation of Silicon substrates with BSA proteins dissolved in Phosphate Buffer Saline. b) Lipid -Dip Pen nanolithography of arbitrary patterns. c) Evaporation of Au sacrificial layer by PVD. d) Lift-off of the lipid masks in the sonication step. e) Sputtering of the desired material. f) Removal of the sacrificial layer. Optical images showing the outcome at key stages (g–j).

As an example, 20 × 20 μm DOPC squares were written on the BSA functionalized surface using L-DPN, as in Figure 2g. In order to create a mold structure ("negative" lithography), a chromium/Au (3 nm/ 20 nm) sacrificial layer was evaporated on top of the sample containing the lipid structures, and shortly after, the lipids were lifted-off by sonicating the sample in acetone for 15 min, which dissolved the lipid structures and part of the BSA underneath lipids. Figure 2h shows the mold that was created after this step (additional examples given as Supporting Information S2). A thin nickel film was then sputtered on top of this mold, to fill the hollow structures, with another 3 nm Cr buffer layer to ensure adhesion (Figure 2i). Finally, the sacrificial Cr/Au layer was lifted-off by 30 min sonication in ethanol (Figure 2j). The effect of two solvents used in the sonication process, namely acetone and ethanol, on the state of the BSA coating was studied more in detail in Section 3 of the Supporting Information. In short, acetone dissolves the lipids and the BSA underneath in the first lift-off step, which ensures that the metallic layer sputtered on the created mold has better adhesion to the substrate, as compared to the first sputtered sacrificial layer, which is peeled off during the second lift-off process, after sonication in ethanol.

This process can be extended to the fabrication of structures of any desired material that can be deposited by PVD. The choice of sputtered materials influences the quality of the lift-off.

In the second lift-off process, which removed the sacrificial layer (Au) (Figure 2f,j), the sonication in the solvent resulted in a lift-off of the Cr and the Au layer, as demonstrated by EDS measurements (Supporting Information S4), locally performed on the obtained Ni square areas.

For simpler patterns, an alternative single-step approach is feasible (Supporting Information S5) where the complementary pattern to the lithographed lipid structure can be printed. ("negative" lithography). This method saves one lithography step, but in return requires longer L-DPN patterning times, as all the areas where a flat substrate is needed have to be covered with ink.

2.2. 3D Lithography

To extend the capabilities of L-DPN from two to three dimensions, we tested how the thickness of the patterned phospholipid layers could be changed by the lithography parameters in a controllable manner. To this goal, the printing of the lipids was done on a BSA-coated substrate and a pristine silicon substrate subsequently, using the same freshly coated probe (see **Figure 3**a–d). Four lines were patterned with increasing writing speed, while keeping the relative humidity constant at 40%. As expected, the patterning on pristine silicon yields the formation of lines of increasing width and roughly the same thickness at slower writing speeds (Figure 3d) as a result of the larger flow of molecules transferred to the substrate and subsequent spreading. In contrast, on BSA-coated surfaces, the reduction of writing speed leads to a remarkable increase in line thicknesses (Figure 3b), up to an order of magnitude bigger as compared to the patterns on pristine Si. The intrinsic ability of BSA to

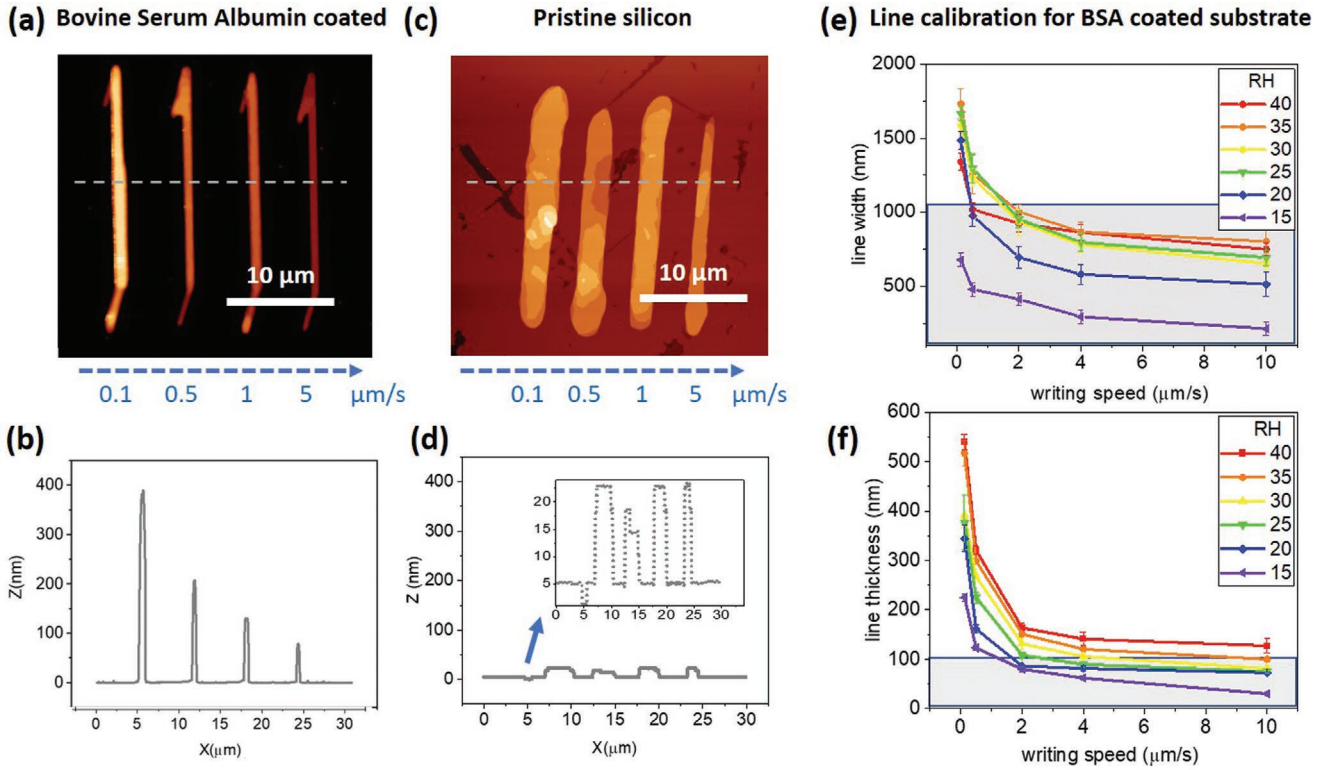

Figure 3. 3D writing of lipids with controlled parameters. a) AFM images of lipid lines written on a BSA-coated substrate with increasing speed and b) corresponding thickness profile. c) Lipid lines written on pristine silicon surfaces under the same writing conditions as in (a) and corresponding thickness profiles in (d). e) Obtained line widths and f) thickness for varying speed and humidity conditions during L- DPN on BSA-coated substrate.

bind fatty acids allowed to write phospholipid patterns with the minimal spreading of lipids. Therefore, by tuning the writing parameters, namely writing speed and relative humidity, the thickness of the written lipid features can be controlled and structures can be patterned in a 3D fashion.

To explore the achievable feature line sizes, systematic experiments were performed by sweeping the relative humidity values and the writing speed on a BSA-coated substrate. The obtained results are displayed in the graphs shown in Figure 3e,f.

The lateral resolution of this approach is given by the average width of the lines. Applying low relative humidity or/and higher writing speeds, fewer lipid molecules flow onto the substrate and sub-micrometer resolution can be achieved. The parameter area where sub-micron resolution can be achieved is highlighted in grey in Figure 3e, and sub-100 nm features have been highlighted in grey in Figure 3f. The decaying curves are characteristic for the dependency of the lipid transport on the relative humidity and writing speed (dwell time) of the process as reported previously.[21] Remarkably, the parameters can be tuned to achieve a wide range of line thicknesses ranging from 50 to 500 nm.

After tuning the thickness of the lipid lines in situ during writing, as a way to generate 3D structures, we set out to explore a nanoscale additive manufacturing process in a layer-by-layer fashion for the lipid system. Here, the question was whether lipid layers can be written on top of each other consecutively (as depicted in **Figure 4**a). Toward this, different structures were patterned onto BSA-coated substrates, with lines or other geometrical shapes (a square, circumference, or circle) written directly on top of a square lipid pattern (Figure 4b), forming 2 or 3-layer structures. We refer the reader to Section 6 of the Supporting Information for further details on the design of these results. A second related experiment was conducted to assess the way the phospholipid layers arrange on top of previously written layers. For this, straight lines were patterned with an increasing number of repetitions/passes. The numerical data shown in Figure 4c,d illustrates how the thickness of the lines increased with every repetition. This occurred in a bigger extent on the first repetitions, but when the number of repetitions is increased, the achieved thickness seems to get closer to a saturation value. Summarizing, the experiments show the feasibility of layer-by-layer writing in L-DPN to generate 3D structures. Such lipid-on-top-of-lipid structures are surprisingly stable for a few days at room temperature, as previous work shows that patterned lipids are prone to spread on hydrophilic surfaces or on top of hydrocarbon chains.[36]

So far, we have presented two different methods to achieve 3D structuring (thickness-tuned writing vs layer-by-layer writing) with L-DPN using lines as building blocks. In order to produce more complex structures; however, shifting to dots as building blocks was more convenient, as we could input a bitmap to the lithography software and write any 3D arbitrary shape by modifying the dot density or the dwell time to achieve control of the lipid thickness parameter.[17] **Table 1** summarizes the approaches that can be applied to achieve 3D writing in L-DPN. As we mentioned before, tuning the writing parameters such as relative humidity and writing speed/dwell time gives

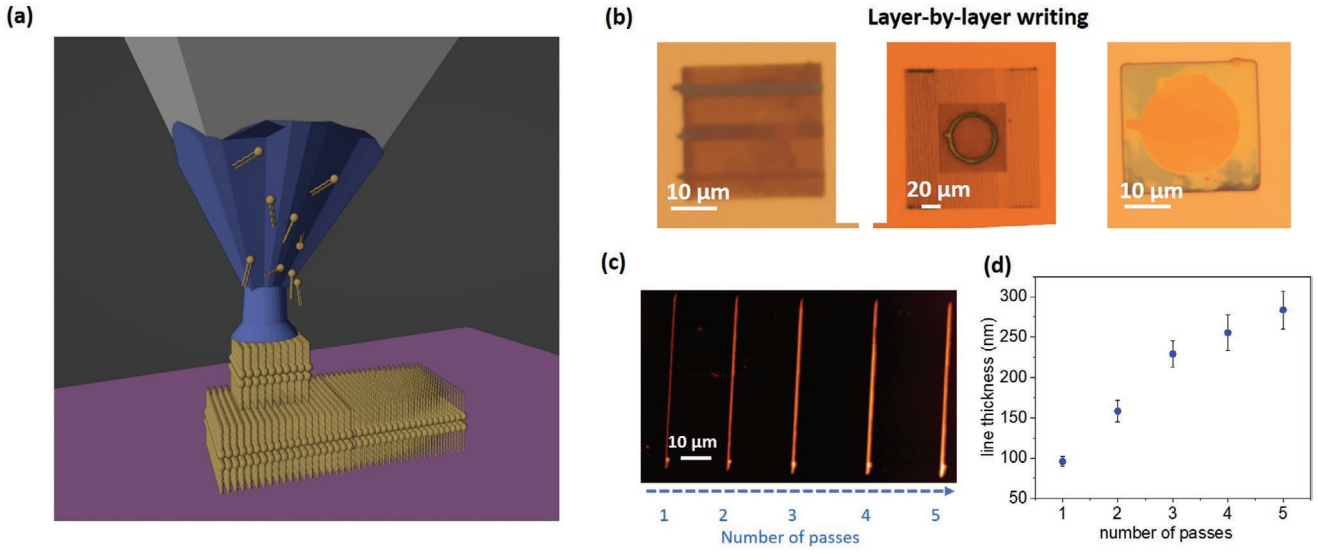

Figure 4. Additive-lipid-layer manufacturing. a) Sketch illustrating the layer-by-layer writing process. b) Examples of 3D structures adding different layers. c) Lipid lines written by increasing number of repetitions and d) corresponding thickness profile measured with AFM.

different lipid thickness values. We showed that we can also leverage an additive manufacturing-based strategy by tuning the density of our building blocks or subsequently adding layers on top of each other.

An example of a more complex structure printed using the "density of dots" approach is displayed in **Figure 5**: an elephant-shaped structure patterned using a dot bitmap. As discussed in Table 1, a higher density of dots gives rise to thicker lipid areas and ultimately yielded a 3D structure.

However, DOPC phospholipid molecules form fluid-phase lipid patches at room temperature, which compromised their usefulness for many applications. For this reason, we explored the metallization approach by PVD as a way to fix the lipid structures (keeping in mind the good stability shown by the lipid structures in high vacuum in the lithography process discussed in Section 2.1). The proposed process is described in Figure 5a. Thus, a 20 nm Au film was evaporated on the sample leading to a now metalized structure (see the sample topography before and after the metallization step in Figures 5c–e). The structure was characterized by AFM before and after the evaporation step, in order to track the changes occurring during the Au deposition. The AFM images and profiles displayed in Figure 5d,f show, that the overall shape of the structure remained unchanged despite the high collision energies to which the lipid patches are subjected. The interaction of the lipids with the Au vapor gave rise to higher surface roughness and we noticed that the edges of the structure are smoothed out, as we see from the overlapping AFM profile images in Figure 5. On the other hand, we noticed that the Au formed a protective layer on the lipid surface that sealed the structure, protecting the lipids from washing off during immersion in water or other solvents and gave lipids long-term integrity (several months), even if the samples were not stored under low humidity conditions. Section 7 of the Supporting Information shows an example of a metalized structure that was measured 9 months after its preparation, showing that despite the structure sinking slightly, it keeps its integrity.

In order to better understand the arrangement of the Au layer on top of the lipid structures, a cross-section was milled using focused ion beam (FIB) and an image of the system was obtained with scanning electron microscopy (SEM). For this purpose, 200 nm thick rectangular lipid structures were freshly prepared and directly coated with a 50 nm Au layer (a thick Au layer was used specifically for better contrast images in SEM). Using FIB milling, 5 µm deep cross-sectional trenches were milled to form a thin lamella (see Supporting Information S8). Prior to this step, a Pt protective layer was deposited in situ using focused ion beam-induced deposition, in order to protect the sample during milling. Remarkably, the lipid structures were not damaged during the process and a cross sectional SEM image was obtained (Figure 5b). The SEM image also showed the created roughness after the evaporation process. The thicker the deposited Au coating, the bigger the roughness, as a result of the increasing number of collision events during PVD. The SEM cross section also revealed that the Au layer was also deposited on the sides of the 3D lipid structures with the same thickness, as a result of the non-directional nature of the thermal evaporation technique. While this contributes to have a protective layer around the whole structure, a lift-off step could still be performed if the necessary energy to break the protective layer is provided through sonication

The presented process for 3D direct writing is low-cost, allows for arbitrary patterns within reasonable time scales (writing speeds of µm s^{-1}), environmentally friendly materials are used and does not require the use of expensive facilities in order to achieve fairly complex 3D structures. A drawback of

Table 1. Different strategies of achieving 3D writing in L-DPN through lines and dots.

	Writing parameters		Lipid stack combination	
Lines	Relative humidity	Writing speed	Line density	Layer-by-layer writing
Dots	Relative humidity	Dwell time	Dot density	Layer-by-layer writing

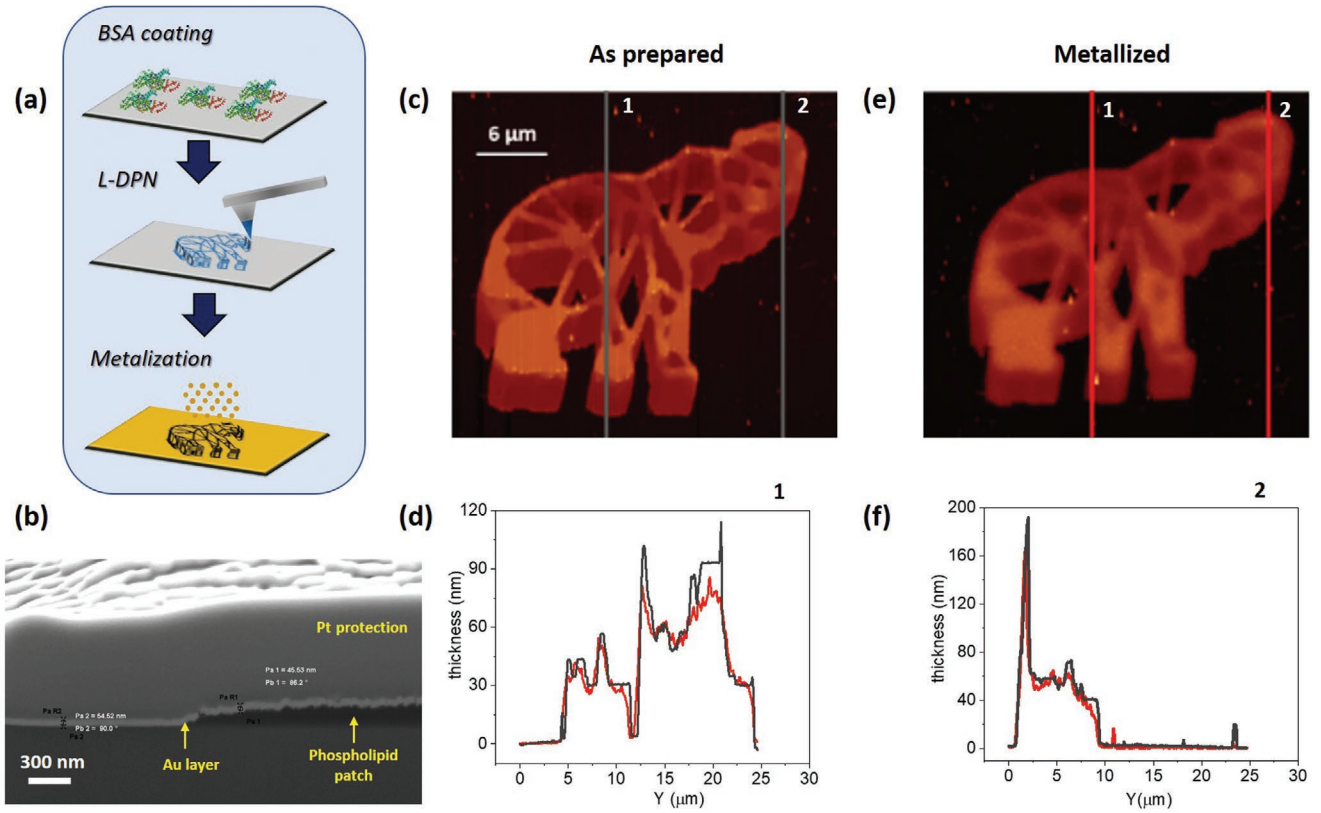

Figure 5. 3D lipid-structure metallization. a) Scheme of the 3D structure fabrication process. b) Cross sectional SEM image of the FIB-milled trench showing the lipids in dark, a 50 nm Au layer, and a thick Pt layer on top. Atomic Force Microscopy image of patterned microscale elephant c) before and e) after the metallization step with corresponding thickness profiles in (d) and (f).

the method is the need to calibrate the lipid ink flow and outcoming layer thickness before producing the desired structures. Controlling the precise amount of the ink loaded onto the tip, in L-DPN, by controlling relative humidity, has a significant impact on the ink flow during the L-DPN process. Optimizing printing processes during L-DPN can facilitate the establishment of highly reproducible and scalable protocols to write on surfaces with specific surface energies. On the other hand, layer-by-layer written structures need to be metalized a few days after fabrication and stored under low humidity to keep the integrity of the samples. However, once metalized, the samples can keep their integrity for several months.

The work presented here is the first step toward the optimization of this approach by using functionalized substrates and controlling the relative humidity and writing speed during L-DPN. Together, controlling those parameters resulted in the fabrication of 3D structures at the nano/micron scale and demonstrated that this approach can be extended to the fabrication of complex 3D structures and its applications in device miniaturization.

3. Conclusion

In the past decade, the advances in lipid membrane patterning have yielded different applications, from biosensors[25,37] to the functionalization of preexisting structures[38] or the nanofabrication of optical structures.[28] In the present work, we have proposed two methods to grow metallic 2D and 3D nanostructures using lipid direct writing with L-DPN. While the typical focus to control the outcome of printing processes at the nanoscale relies on designing the ink, we propose to work on the substrate properties in a way that the ink molecules are anchored to the surface where they are printed. We demonstrate that by leveraging the strong binding between the BSA protein (on the substrate) and the phospholipids (as ink), we can conduct facile processes to create 2D structures of arbitrary shape and material, that require no special infrastructure facilities as clean rooms or expensive lithography equipment, like electron beam lithography. Moreover, the capabilities of L-DPN are extended from 2D to 3D writing, either by controlling the thickness dimension during writing through the writing parameters or by implementing a layer-by-layer writing process. The integrity of the phospholipid patches at low-pressure conditions and during energetic processes such as PVD is very high and proven throughout the experiments shown in the manuscript. All in all, this works pushes the limits of low-cost nanofabrication, introducing an original bioinspired approach to create 3D structures.

4. Experimental Section

Functionalization of the Substrates: Si substrates were cleaned by consecutive sonication in acetone, ethanol, and DI water and dried under nitrogen flow. BSA was purchased from Sigma Aldrich (Germany). It was dissolved in Phosphate Buffer Saline in a (10:90) vol.% ratio. And

directly used to incubate freshly cleaned Si substrates for 1 h, at room temperature (RT). The substrates were then rinsed with deionized water, to remove the salt from the surface, dried under nitrogen flow, and stored at RT until used.

Preparation of Phospholipid Inks: The DOPC dissolved in a chloroform 20 mg ml^{-1}, was purchased from Avanti Polar Lipids (USA).

Dip-Pen Nanolithography: The lipid writing was carried out on an NLP2000 system (NanoInk, USA) with A-type cantilevers and a matching ink reservoir (NanoInk). The inkwells were loaded with 1 µL ink solution and then allowed to evaporate the solvent (chloroform) in the air for a few minutes. Wetting the probes with ink was performed by dipping it in the inkwells channel for 15 min at high humidity (80% RH). Before writing on the substrates, the excess ink was removed from the tip by writing on a sacrificial area. Notice that this is a critical step to achieve homogeneity, in particular, for the 3D printed structures. Typical writing parameters range between 30–40% relative humidity and a writing speed between 0.1 and 5 µm s^{-1}.

Physical Vapor Deposition: Sacrificial layers of Au of 20–50 nm were evaporated using a home-built e-beam evaporation system, setting the pressure to 10^{-7} mbar with an evaporation rate of 0.08 nm s^{-1}. A 3 nm chromium buffer layer was grown previously to improve the adhesion of Au.

The Chromium/Ni layers were deposited on a prepared Au mold using a home-built magnetron sputtering system from pure Cr and Ni (99.99% purities) 3-inch targets. The distance from targets to substrate was 290 mm with a tilt angle of 37.5° relative to the *z*-axis. The base pressure before the deposition was lower than 1.1×10^{-9} mbar. The working pressure and flow rate of Ar were kept constant at 3×10^{-3} mbar and 40 sccm, respectively. The substrate was continuously rotated at 20 rpm to improve the homogeneity of the film. Cr-layer was deposited for 1.5 min using a power of 90 W, resulting in an approximate thickness of 3 nm. Ni-layer was deposited for 34 min with a power of 30 W, resulting in an approximate thickness of 25 nm.

Lift-Off of the Phospholipid Patterns: To create the molds, the lithographed lipid patches, used as resists, were lifted-off by 15 min of sonication in acetone. The samples were then rinsed in ethanol and water and dried under nitrogen flow.

Etching of the Sacrificial Layer: The sacrificial Au layer was etched by sonicating the sample for 30 min in ethanol solution.

Contact-Angle Measurements: BSA-coated surfaces were characterized via contact angle measurements on an OCA-20 system (DataPhysics Instruments GmbH, Filderstadt, Germany), by the sessile drop method. Droplets with a volume of 2.0 µL were deposited at different locations at room temperature (RT). The contact angles were determined with the onboard software.

Optical Imaging: Fluorescence microscopy images were obtained on a Zeiss set-up equipped with SARFUS Software (Nanolane).

Atomic Force Microscopy Imaging: AFM images were performed on a Dimension Icon system (Bruker, Germany). Measurements in the air were done in amplitude modulation mode with a 40 N m^{-1} probe from Budgetsensors, setting a typical oscillation amplitude of 10 nm. The data was analyzed using the WSxM software.[39]

Energy Dispersive X-Ray Spectroscopy: The chemical composition of the samples was studied using an SEM LEO-1530 equipped with an energy dispersive spectroscopy (EDS) detector (AZTEC-System, Oxford Instruments, UK). The acceleration voltage and the working distance were 10 kV and 8.5 mm, respectively.

Focus Ion Beam Milling and Scanning Electron Microscopy Imaging: To inspect the cross section of the lipid patches coated with an Au layer, FIB milling, and subsequent SEM measurements were performed in a dual beam Auriga 60 system (Zeiss, Germany). With a 30 kV Ga-ion beam, 5 µm of depth milling was conducted with 30 kV and 600 pA of milling current at −50°C, using a Deben 2020A Ultra cryo-stage.

Supporting Information

Supporting Information is available from the Wiley Online Library or from the author.

Acknowledgements

E.B. acknowledges the Karlsruhe Institute of Technology for a postdoctoral fellowship in the frame of the YIG Prep Pro program and the Spanish Ministry of Science for a Juan de la Cierva Incorporation fellowship. This work was carried out with the support of the Karlsruhe Nano Micro Facility (KNMF, www.knmf.kit.edu), a Helmholtz Research Infrastructure at Karlsruhe Institute of Technology (KIT, www.kit.edu). M.H. acknowledges additional support by the Helmholtz Association in the form of a Helmholtz ERC Recognition Award.

Open access funding enabled and organized by Projekt DEAL.

Conflict of Interest

The authors declare no conflict of interest.

Data Availability Statement

The data that support the findings of this study are available from the corresponding author upon reasonable request.

Keywords

3D printing, bovine serum albumin (BSA), dip-pen nanolithography, lipids, nanostructuring, scanning probe lithography

Received: September 9, 2022
Revised: November 30, 2022
Published online:

[1] Y. Chen, Z. Shu, S. Zhang, P. Zeng, H. Liang, M. Zheng, H. Duan, *Int. J. Extreme Manuf.* **2021**, *3*, 032002.
[2] J. S. O. Neill, P. Salter, Z. Zhao, B. Chen, H. Daginawalla, M. J. Booth, S. J. Elston, S. M. Morris, *Adv. Opt. Mater.* **2022**, *10*, 2102446.
[3] R. F. Hamans, J. Liao, A. Welbourne, R. Lavrijsen, A. Fernandez-Pacheco, *ACS Nano* **2017**, *11*, 11066.
[4] M. Jaafar, J. Pablo-navarro, E. Berganza, P. Ares, C. Magén, A. Masseboeuf, C. Gatel, E. Snoeck, J. Gómez-herrero, J. M. De Teresa, A. Asenjo, *Nanoscale* **2020**, *12*, 10090.
[5] Y. Yang, K. W. Leong, *Wiley Interdiscip. Rev.: Nanomed. Nanobiotechnol.* **2010**, *2*, 478.
[6] T. Abele, T. Messer, K. Jahnke, M. Hippler, M. Bastmeyer, M. Wegener, K. Göpfrich, *Adv. Mater.* **2021**, *34*, 2106709.
[7] M. Hippler, K. Weißenbruch, K. Richler, E. D. Lemma, M. Nakahata, B. Richter, C. Barner-Kowollik, Y. Takashima, A. Harada, E. Blasco, M. Wegener, M. Tanaka, M. Bastmeyer, *Sci. Adv.* **2020**, *6*, abc2648.
[8] S. He, R. Tian, W. Wu, W. Li, D. Wang, *Int. J. Extreme Manuf.* **2021**, *3*, 012001.
[9] C. Donnelly, A. Hierro-rodríguez, C. Abert, K. Witte, L. Skoric, D. Sanz-hernández, S. Finizio, F. Meng, S. Mcvitie, J. Raabe, D. Suess, R. Cowburn, A. Fernández-pacheco, *Nat. Nanotechnol.* **2022**, *17*, 136.
[10] J. Hengsteler, B. Mandal, C. Van Nisselroy, G. P. S. Lau, T. Schlotter, T. Zambelli, D. Momotenko, *Nano Lett.* **2021**, *21*, 9093.
[11] F. Meng, C. Donnelly, L. Skoric, A. Hierro-Rodriguez, J. Liao, A. Fernandez-Pacheco, *Micromachines* **2021**, *12*, 859.
[12] A. May, M. Saccone, A. Van Den Berg, M. Hunt, S. Ladak, *Nat. Commun.* **2021**, *12*, 3217.
[13] L. Yang, F. Mayer, U. H. F. Bunz, E. Blasco, M. Wegener, *Light: Adv. Manuf.* **2021**, *2*, 17.

[14] J. Ventrici de Souza, Y. Liu, S. Wang, P. Dörig, T. L. Kuhl, J. Frommer, G. Liu, *J. Phys. Chem. B* **2018**, *122*, 956.
[15] E. Berganza, G. Apte, S. K. Vasantham, T. Nguyen, *Polymers* **2022**, *14*, 1327.
[16] T. G. Pattison, S. Wang, R. D. Miller, G. Liu, G. G. Qiao, *Nat. Commun.* **2022**, *13*, 1941.
[17] G. Liu, M. Rong, H. Hu, L. Chen, Z. Xie, Z. Zheng, *Adv. Mater. Technol.* **2022**, *7*, 2101493.
[18] E. Berganza, M. Hirtz, *ACS Appl. Mater. Interfaces* **2021**, *13*, 50774.
[19] X. Liu, C. Carbonell, A. Braunschweig, *Chem. Soc. Rev.* **2016**, *45*, 6289.
[20] S. Lenhert, P. Sun, Y. Wang, H. Fuchs, C. A. Mirkin, *Small* **2007**, *3*, 71.
[21] A. Urtizberea, M. Hirtz, *Nanoscale* **2015**, *7*, 15618.
[22] A. Urtizberea, M. Hirtz, H. Fuchs, *Nanofabrication* **2015**, *2*, 43.
[23] A. E. Kusi-Appiah, N. Vafai, P. J. Cranfill, M. W. Davidson, S. Lenhert, *Biomaterials* **2012**, *33*, 4187.
[24] S. Sekula, J. Fuchs, S. Weg-Remers, P. Nagel, S. Schuppler, J. Fragala, N. Theilacker, M. Franzreb, C. Wingren, P. Ellmark, C. A. K. Borrebaeck, C. A. Mirkin, H. Fuchs, S. Lenhert, *Small* **2008**, *4*, 1785.
[25] H. Y. Liu, R. Kumar, C. Zhong, S. Gorji, L. Paniushkina, R. Masood, U. A. Wittel, H. Fuchs, I. Nazarenko, M. Hirtz, *Adv. Mater.* **2021**, *33*, 2008493.
[26] U. Bog, T. Laue, T. Grossmann, T. Beck, T. Wienhold, B. Richter, M. Hirtz, H. Fuchs, H. Kalt, T. Mappes, *Lab Chip* **2013**, *13*, 2701.
[27] S. Biswas, F. Brinkmann, M. Hirtz, H. Fuchs, *Nanofabrication* **2015**, *2*, 19.
[28] S. Lenhert, F. Brinkmann, T. Laue, S. Walheim, C. Vannahme, S. Klinkhammer, M. Xu, S. Sekula, T. Mappes, T. Schimmel, H. Fuchs, *Nat. Nanotechnol.* **2010**, *5*, 275.
[29] M. Hirtz, A. Oikonomou, T. Georgiou, H. Fuchs, A. Vijayaraghavan, *Nat. Commun.* **2013**, *4*, 2591.
[30] M. Hirtz, A. Oikonomou, N. Clark, Y. Kim, H. Fuchs, A. Vijayaraghavan, *Nanoscale* **2016**, *8*, 15147.
[31] M. Gavutis, V. Navikas, T. Rakickas, S. Vaitekonis, R. Valiokas, *J. Micromech. Microeng.* **2016**, *26*, 025016.
[32] H.-Y. Liu, R. Kumar, M. Takai, H. Michael, *Molecules* **2020**, *25*, 2768.
[33] A. A. Spector, *J. Lipid Res.* **1975**, *16*, 165.
[34] J. B. Swaneyf, I. M. Klotz, *Biochemistry* **1970**, *9*, 2570.
[35] J. G. Vilhena, P. Rubio-pereda, P. Vellosillo, P. A. Serena, *Langmuir* **2016**, *32*, 1742.
[36] M. Hirtz, A. Oikonomou, S. Varey, H. Fuchs, A. Vijayaraghavan, in *Microscopy and Microanalysis*, Cambridge University Press, Cambridge, UK **2014**, pp. 2058.
[37] E. Berganza, M. P. Ebrahimkutty, S. Vasantham, C. Zhong, A. Wunsch, A. Navarrete, M. Galic, M. Hirtz, *Nanoscale* **2021**, *13*, 12642.
[38] U. Bog, F. Brinkmann, S. F. Wondimu, *Adv. Sci.* **2015**, *2*, 1500066.
[39] I. Horcas, R. Fernández, J. M. Gómez-Rodríguez, J. Colchero, J. Gómez-Herrero, A. M. Baro, *Rev. Sci. Instrum.* **2007**, *78*, 013705.